J. Fluid Mech. (1978), *vol.* 84, *part* 3, *pp.* 455–469
Printed in Great Britain

The physics of vortex-ring evolution in a stratified and shearing environment

By J. C. S. MENG

Science Applications, Inc., P.O. Box 2351, La Jolla, California 92037

(Received 4 January 1977)

A semi-analytical numerical study was performed to simulate the development of a vortex ring in a stratified and/or shearing environment. Practical applications of results of this study can be found in turbulence modelling and in studies of plumes and wakes. The objective is to follow exactly the evolution of a vortex ring so that the three-dimensional vortex-stretching mechanisms due to stratification and the shear effects, respectively, can be understood.

The basic formulation consists of the solution of the vorticity equation in a stratified medium. The approach adopted is unique in that discrete vortex elements are used and arbitrary nonlinear interactions are allowed (therefore three-dimensional effects) among various vorticity generators. One of the two fundamental assumptions in this approach is that the vorticity is allowed to be generated only along the density discontinuity. The second assumption is that, while the vorticity carried by the vortex ring is modelled by vortex elements tangential to the vortex loop (which was a vortex ring initially), the vorticity generated by stratification effects is modelled by long vortex lines parallel to the axis of the vortex ring. This limits the validity of the present calculation to high Froude number flow.

Numerical stability is guaranteed by the finite core radius for each discrete vortex element and uniform spacing between them; the former is determined by consideration of the momentum integral over the vortex-ring plane. The latter is determined by a cubic spline interpolation method which conserves the circulation and centroids of the vorticity. The velocity of each vortex element is determined by the discretized Biot–Savart law, and motion of the vortex loop is calculated by a predicator–corrector time integration method.

Calculations were carried out for both momentum-carrying and momentumless vortex rings. A particular two-dimensional case gives good agreement with Kármán's theory. The evolution of the vortex loop reveals a process in which only the vorticity normal to the stratification is conserved; the remaining vorticity is dissipated through a simulated viscous dissipation. Evolution of a vortex loop on a shear layer reveals a vortex-loop rotation rate equal to the velocity shear, and a twisting motion due to the Magnus force which can lead to the turbulence energy cascade phenomenon. Numerical results demonstrate effects of each individual vorticity source and observed phenomena can be explained.

1. Introduction

It is well known in turbulence theory that energy is transferred from large to small scales through the three-dimensional vortex-stretching mechanism. Although many explanations have been given (Tennekes & Lumley 1972, p. 91), there seems to be little quantitative support. It has also long been understood that jets and wakes can be idealized by a series of vortex rings, but few studies have been carried out in terms of three-dimensional vorticity theory. In a shearing environment, the Magnus force plays a role which can only be studied numerically. In a stratified medium, the three-dimensional vortex-stretching mechanism is further complicated by the fact that the stratified medium can generate vorticity as soon as it is disturbed from its equilibrium position.

The objectives of this study are first to demonstrate the effects of stratification and shear on a single vortex ring, then to identify the basic physical forces present and finally, perhaps, to shed some light on the turbulence decay process and the evolution of plumes, jets and wakes in a stratified and shearing environment.

The basic approach applied here is to solve the vorticity equation in a stratified medium. For high Reynolds number flows, the diffusion time l^2/ν, where ν is the kinematic viscosity and l is any length scale, is long relative to the time interval of interest. Vorticity is concentrated in isolated rotational flow regions, which can therefore be idealized as discrete vortex elements. The numerical approach adopted here is unique in that discrete vortex elements are used and arbitrary nonlinear interactions among various vorticity generators (and therefore three-dimensional effects) are allowed.

Historically, the first such numerical calculation using a two-dimensional discrete vortex element method was made by Rosenhead (1931). Since then, the same method has been applied to various shear flows and is summarized in a literature survey by Fink & Soh (1974). Of these flows, the major ones are two-dimensional turbulence (Chorin 1973), three-dimensional laminar flows (Leonard 1974; 1975, private communication) and stratified flows in both homogeneous and porous media (Thomson & Meng 1974).

The basic advantage of the discrete vortex element method over the finite-difference method for solving high Reynolds number shear and stratified flows is as follows. The method lends itself to simulation of flows of arbitrarily high Reynolds number. It eliminates the necessity to solve for the irrotational flow domain, which remains passive. It provides the capability for simulating arbitrary stratification effects, i.e. it can simulate the limiting case of a sharp density interface and it eliminates the Courant–Friedrichs–Lewy (CFL) condition, which imposes a time-step limitation based upon the arbitrarily chosen mesh size instead of the physical time scale based upon vortex interactions.

One of the two fundamental assumptions in this approach is that vorticity is allowed to be generated only along the density discontinuity. The second assumption is that while the vorticity carried by the vortex ring is modelled by vortex elements tangential to the vortex loop (which was a vortex ring initially), the vorticity generated by stratification effects is modelled by long vortex lines parallel to the axis of the vortex ring. This limits the validity of the present calculation to high Froude number flow.

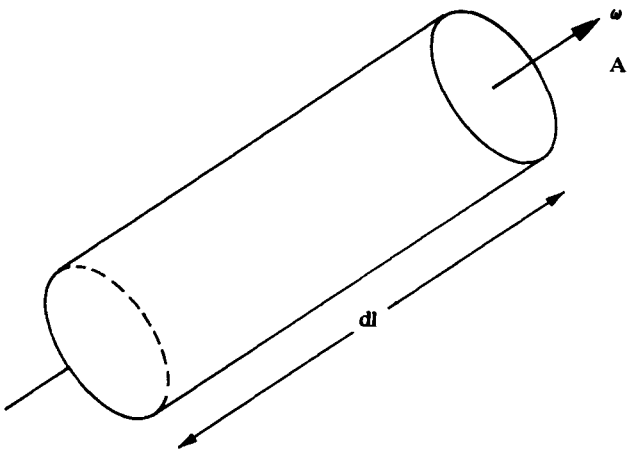

FIGURE 1. A vortex line element.

Numerical stability is guaranteed by the finite core radius r_c for each discrete vortex element and by uniform spacing between them; the former is determined by consideration of the momentum integral over the vortex-ring plane. The latter is determined by a cubic spline interpolation method which conserves the circulation and centroids of the vorticity. The velocity of each vortex element is determined by the discretized Biot–Savart law, and motion of the vortex loop is calculated by a predicator–corrector time integration method.

Calculations were carried out for both momentum-carrying and momentumless vortex rings. The finite core radius was chosen to match the fluid velocity profile in the wake of a towed body for the first case and, similarly, to match the wake profile of a self-propelled body for the second case. In a stratified medium, the evolution of the vortex loop reveals a process in which only the vorticity normal to the stratification is conserved; the remaining vorticity is reduced once the separation distance between opposite sides of the vortex loop falls within the core radius. Without stratification, evolution of the vortex loop on a shear layer reveals a vortex-loop rotation rate equal to the velocity shear, and a twisting motion due to the Magnus force which can lead to the energy cascade phenomenon of turbulence theory. In either case, the vortex loop is 'collapsed' and forms 'tip vortices'. For the two-dimensional stratification but without shear, the growth rate of the vortex loop agrees with both Kármán's theory and Wu's experimental data.

2. Formulation

2.1. *Basic physical modelling*

The fundamental approximations made in this numerical study are that the flow is inviscid and incompressible and the Boussinesq approximation is applicable, that the discontinuous density interface is identifiable by vortices and stratification effects may be modelled by infinitely long vortex lines for the case $F_D = U/ND \gg 1$, and finally, that turbulent diffusion affects the vortex core structure only.

Since the common vortex interaction mechanism is well described in the literature,

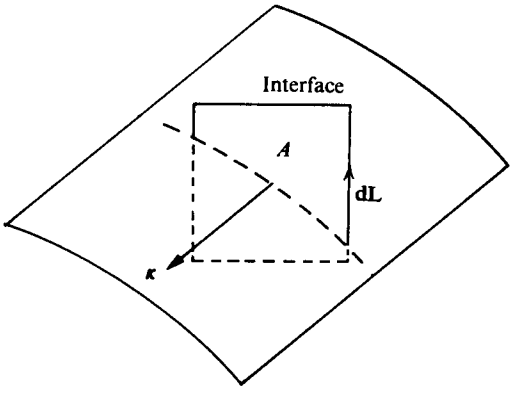

FIGURE 2. A vortex line element lying on a density interface.

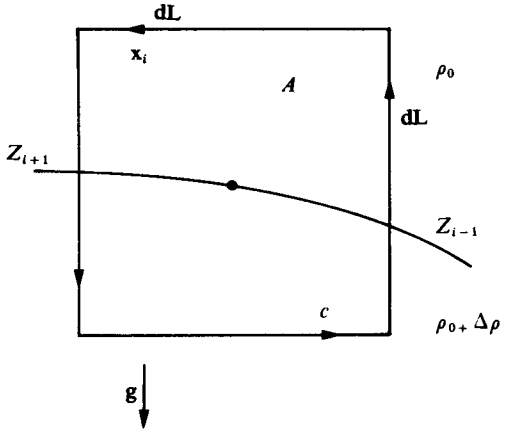

FIGURE 3. Geometric relationship between the rate of change of circulation and the slope of the interface.

we shall concentrate only on the added feature of this study, i.e. the modelling of the stratified flow in terms of discrete vortex elements.

In stratified flow, vorticity varies not only as a result of vortex stretching and turbulent diffusion, but also owing to the density stratification; therefore the circulation carried by vortex lines is no longer constant as it is in a non-stratified medium according to Kelvin's theorem. To derive the time rate of change of the vortex-line circulation, we begin with the following set of equations:

$$d\boldsymbol{\omega}/dt = -\nabla \times (\rho^{-1}\nabla p) + (\boldsymbol{\omega}.\nabla)\mathbf{u} + \nu\nabla^2\boldsymbol{\omega}, \tag{1}$$

$$\nabla.\mathbf{u} = 0, \quad \nabla p \cong \rho_0 \mathbf{g}. \tag{2),(3}$$

Defining the circulation along the infinitely long vortex lines as $\kappa = \boldsymbol{\omega}.\mathbf{A}$, where $\mathbf{A}$ is the elemental area normal to $\boldsymbol{\omega}$ (figure 1), we find the time rate of change of κ from the equation

$$\frac{d\kappa}{dt} = \mathbf{A}.\frac{d\boldsymbol{\omega}}{dt} + \boldsymbol{\omega}.\frac{d\mathbf{A}}{dt}. \tag{4}$$

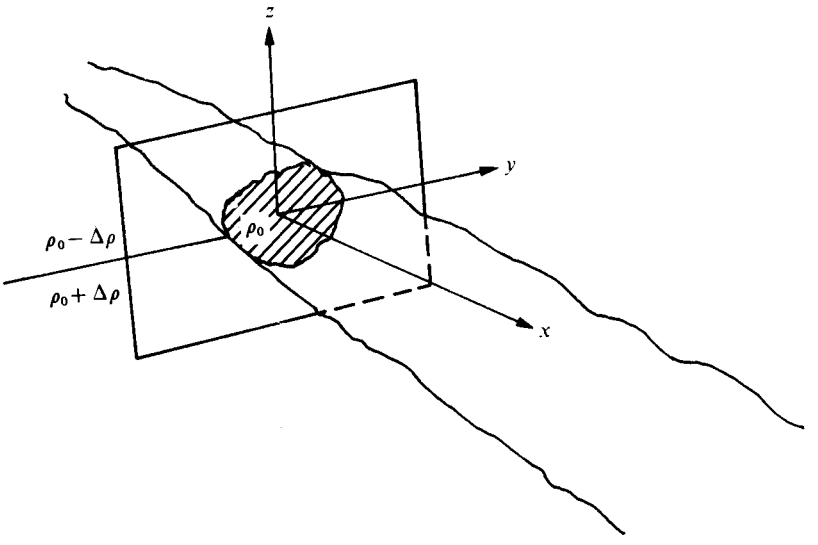

FIGURE 4. Co-ordinate system for the case of a wake on a sharp thermocline.

The first term can be obtained by multiplying (1) by **A** and the second term by invoking the incompressibility condition. Figure 1 shows a vortex element of area **A** and length **dl**; the fluid volume **A**.**dl** contained in the tube should be constant with respect to time, i.e. $\mathbf{dl}.(\mathbf{dA}/dt) = -\mathbf{A}.(d\mathbf{dl}/dt)$, so that $\boldsymbol{\omega}.(d\mathbf{A}/dt) = -(\kappa/dl)d(dl)/dt$. Then the last term in (4) is simply the stretching term, i.e. $(\boldsymbol{\omega}/dl)d(dl)/dt \equiv (\boldsymbol{\omega}.\nabla)\mathbf{u}$. This equation and (1) reduce (4) to

$$d\kappa/dt = -\mathbf{A}.\nabla\times(\rho^{-1}\nabla p) + \nu\mathbf{A}.\nabla^2\boldsymbol{\omega}. \tag{5}$$

For convenience, we can rewrite (5) in a slightly different form. Take an interface (see figure 2) on which the vortex line $\boldsymbol{\kappa}$ lies where the elemental area is denoted by a vector **A** parallel to $\boldsymbol{\kappa}$; if we look along $\boldsymbol{\kappa}$, we have figure 3. A portion of **A** lies in a medium with density $\rho_0 + \Delta\rho$; the remaining, upper portion has density ρ_0. Applying (5) over the area A and neglecting diffusion, we then have

$$\frac{d\kappa}{dt} = -\int_A d\mathbf{A}.\nabla\times\left(\frac{1}{\rho}\nabla p\right),$$

or by Stokes' law

$$\frac{d\kappa}{dt} = -\oint_c \left(\frac{1}{\rho}\nabla p\right).\mathbf{dL}, \tag{6}$$

where the contour c is followed anticlockwise. If the fluid is assumed to be in hydrostatic equilibrium so that $\nabla p \cong \rho_0\mathbf{g}$, then

$$\frac{d\kappa_i}{dt} = -\oint\frac{\rho_0}{\rho}\,\mathbf{g}.\mathbf{dL} \cong g\frac{\Delta\rho}{\rho_0}(Z_{i+1} - Z_{i-1}), \tag{7}$$

which is the equation necessary for advancing the circulations κ_i.

2.2. *Formulation of the numerical procedure*

In this subsection we shall outline the numerical procedure for finding the motion of vortex loops in a stratified medium for the case $F_D \gg 1$. If the vortex loop is taken as

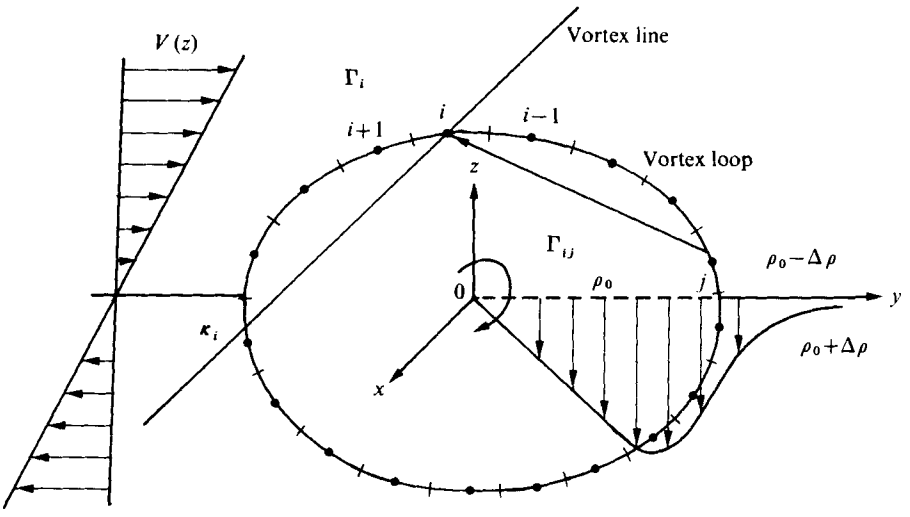

FIGURE 5. Discretization of a vortex loop on a sharp thermocline.

the boundary of the cross-section of a wake or jet, figure 4 illustrates the co-ordinate systems and the idealized physical problem.

Figure 5 shows a vortex loop located on a sharp thermocline with constant density inside the loop and with an ambient density which differs by $2\Delta\rho$ above and below the thermocline. The vortex loop is discretized into N elements identified by the index i and each containing a circulation $\mathbf{\Gamma}_i$ along the loop. The velocity of each element due to the vortex loop can then be calculated from

$$\mathbf{u}_i = -\frac{1}{4\pi}\sum_{j,\,j\neq i}^{N}\frac{\mathbf{\Gamma}_j\times\mathbf{r}_{ij}}{(\mathbf{r}_{ij})^3}\,dl_j, \tag{8}$$

where dl_j is the length of element j and $\mathbf{r}_{ij}$ is the vector connecting elements i and j. Additional contributions to this velocity come from all other straight and infinitely long ($F_D \gg 1$ case) vortex lines which pass through the vortex loop at nodes $\mathbf{x}_i$. The circulation carried by those vortex lines is denoted by $\boldsymbol{\kappa}_i = \kappa_i(1,0,0)$, i.e. they have circulation along the vortex-loop axis only, and the additional velocity contribution can be calculated from

$$-\frac{1}{2\pi}\sum_{j,\,j\neq i}^{N}\frac{\boldsymbol{\kappa}_j\times\mathbf{r}_{ij}}{(\mathbf{r}_{ij})^2}, \tag{9}$$

where the $\boldsymbol{\kappa}_i$ are obtained from

$$\frac{d\kappa_i}{dt} = g\frac{\Delta\rho}{\rho_0}\Delta Z_i, \quad \Delta Z_i = \tfrac{1}{2}(Z_{i+1}-Z_{i-1}).$$

The last two relations were derived in (7). With these equations, the vortex-loop and vortex-line position can be updated and the entire process can be repeated over the time period of interest.

2.3. *Formulation of the finite core radius*

It was pointed out by Chorin (1973) that, unless a finite core radius is incorporated, the accuracy of the discrete vortex element method does not improve with an incre-

ment of the total number of vortex elements. The finite core radius employed in the present study uses an algebraic relation which not only satisfies the physical smoothing requirement, but also eliminates a test to find out whether the point of concern falls within the core radius or not.

The denominator in the velocity relation (9) is modified by replacing $|\mathbf{r}_{ij}|^2$ by $|\mathbf{r}_{ij}|^2+r_c^2$, where r_c is the core radius. For $|\mathbf{r}_{ij}| \ll r_c$, and therefore in the core, the velocity grows linearly with respect to the distance $|\mathbf{r}_{ij}|$ but falls off as $1/|\mathbf{r}_{ij}|$ if $|\mathbf{r}_{ij}| \gg r_c$. Similarly, the denominator in the three-dimensional relation (8) is replaced by $|\mathbf{r}_{ij}|^3+r_c^3$, so that

$$|\mathbf{u}_i| \sim \begin{cases} \Gamma|\mathbf{r}_{ij}| & \text{for} \quad |\mathbf{r}_{ij}| \ll r_c, \\ \Gamma/|\mathbf{r}_{ij}|^2 & \text{for} \quad |\mathbf{r}_{ij}| \gg r_c. \end{cases}$$

2.4. *Formulation of the reseeding procedure*

One problem which is commonly associated with a Lagrangian calculation is the continual addition or removal of particles from the calculation. Depending upon the physical nature of the problem, particles may accumulate and yield unrealistically high gradients of flow variables or the number of particles in a region of interest may become so low that no realistic representation of the flow is possible. From the point of view of maintaining a uniform accuracy, a reseeding procedure which can rearrange, add or delete particles as necessary must be applied. It is also desirable from an economic point of view since a number larger than a limiting number of vortices will not improve accuracy, but a number smaller than a limiting number of vortices will reduce accuracy. Without being committed to using a large number of particles throughout the computation, there is no alternative but to adopt a reseeding procedure. Since the vortices do carry physical variables (vorticity) the reseeding procedure must be based upon the laws of conservation. For the present method, the quantities conserved are the vorticity and the centroid of the vorticity.

The method adopted here is to impose an equal separation distance between the vortices at all times. This separation distance can either be constant or vary as a function of time. Then the vortices are rearranged according to this requirement and the physical variables, circulation and spatial positions are interpolated using a cubic spline interpolation polynomial over all the vortices. Through numerical experiments which will be discussed in § 3, it is evident that this reseeding procedure is effective in removing 'spurious' numerical errors. The reason for the success of using an 'equal separation distance' between the discrete vortex elements is explained in Fink & Soh (1974).

The conservation laws are well satisfied since the interpolation procedure interpolates over all the vortices at once. Naturally, the centroid of the circulation is also an invariant if the circulation profile is not altered by the spline fit.

3. Results and discussion

3.1. *Initiation of the calculation*

Assuming that the interior of the vortex loop, which can be imagined to be a jet or wake, is of constant density and that the vortex loop is located on a thermocline as shown in figures 4 and 5, the density differs by $\Delta\rho$ between the interior and the exterior

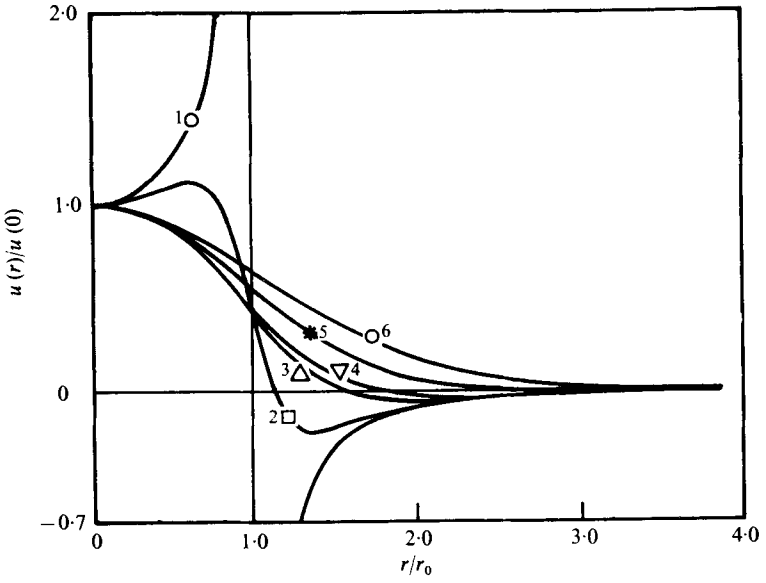

FIGURE 6. Effects of core radius on the velocity profile generated by a vortex ring. —①—, $\bar{r}_c = 0$; —②—, $\bar{r}_c = 0{\cdot}3$; —③—, $\bar{r}_c = 0{\cdot}8$; —④—, $\bar{r}_c = 1{\cdot}0$; —⑤—, $\bar{r}_c = 1{\cdot}5$; —⑥—, $\bar{r}_c = 2{\cdot}0$.

ambient state. The infinitely long vortex lines are drawn from the loop to simulate the vorticity generated by the density stratification; initially these long vortex lines carry no circulation.

To initiate the calculation, Γ_i and its location are required. Assuming the vortex loop to be a vortex ring initially, we can calculate the velocity on the vortex-ring plane from the following integral:

$$u(r) = \frac{\Gamma}{2\pi r_0}\int_0^{\pi} \frac{(1-a\cos\theta)\,d\theta}{(1-2a\cos\theta+a^2+\bar{r}_c^2)^{\frac{3}{2}}},$$

where Γ is the undetermined circulation, r_0 the ring radius, $a = r/r_0$ and θ is the azimuthal angle around the vortex-ring axis. The unknowns are the core radius $\bar{r}_c = r_c/r_0$, Γ and r_0, and can be determined from the following conditions:

(i) The velocity at the vortex-ring centre should be matched to a jet or wake velocity profile.

(ii) For the momentumless case, the integral

$$\int_0^{\infty} u(r)\,r\,dr = 0$$

must be satisfied.

(iii) r_0 is approximately the propeller radius for the wake of a self-propelled body, the jet radius for a jet or the body radius for the wake of a towed body.

A calculation was carried out to determine those parameters. Figure 6 shows the effect of the core radius on the velocity profile $u(r)$ normalized by $u(0)$ on the vortex axis. For the case $\bar{r}_c \equiv 0$, the velocity diverges near the centre of the vortex ring, as expected, and too small a core radius results in an unrealistic velocity profile. It was found that $\bar{r}_c = 0{\cdot}8$ yields the best profile for a momentumless case and $\bar{r}_c$ is set to be $0{\cdot}8$ henceforth for the momentumless calculation. Similarly, one finds that $\bar{r}_c = 2$

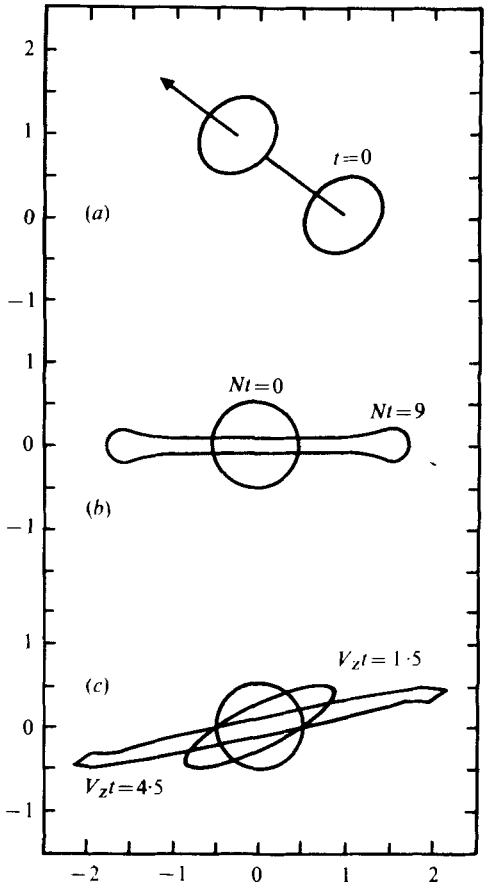

FIGURE 7. Configurations of the vortex loop as a function of time t. N is the Brunt–Väisälä frequency, V_Z is the cross-shear. (*a*) With circulation, viewed at an angle, $\Gamma \neq 0$, $N = 0$, $V_Z = 0$, $\Gamma t/D^2 = 14{\cdot}4$. (*b*) With density stratification, viewed along the axis of the vortex ring, $N \neq 0$, $\Gamma = 0$, $V_Z = 0$. (*c*) With cross-shear, viewed along the axis of the vortex ring, $V_Z \neq 0$, $\Gamma = 0$, $N = 0$.

yields the wake velocity profile for a towed body, or conversely, the velocity profile of a jet. For all the cases reported here, we have used a core radius $\bar{r}_c = 0{\cdot}8$.

3.2. *Numerical results*

Numerical calculations were performed for both momentum-carrying and momentumless vortex loops to simulate wakes generated by towed or self-propelled bodies. Results of these calculations can be directly carried over to jets; only the sense of the vorticity is reversed. Since the vortex-loop representation of the wake of a towed body differs from that of a self-propelled body only in the core radius, in this study we shall concentrate on momentumless vortex loops, i.e. the wake of a self-propelled body.

With the set of initial conditions chosen in the last section, we have carried out three sample calculations to demonstrate individual effects of the circulation Γ, density stratification N and cross-shear V_Z. Results are shown and discussed in

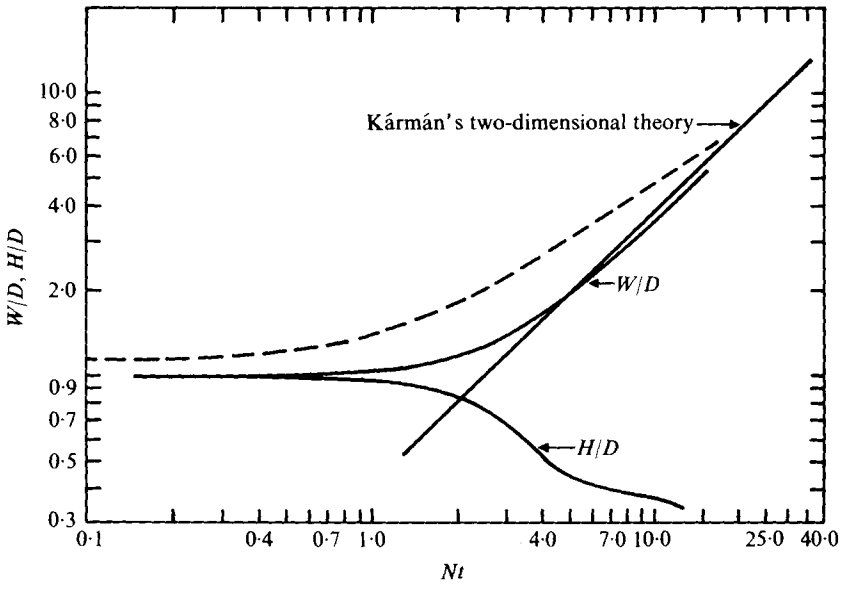

FIGURE 8. Width and height of a collapsing constant-density mixed region in a stably stratified medium. ——, numerical result; – – – –, experimental data (Wu 1969).

§3.2.1. Section 3.2.2 discusses the formation of 'tip vortices' for a circulation-carrying vortex loop in either a stratified or a cross-shear environment. Section 3.2.3 describes the wake rotation as a result of the cross-shear vortex loop.

3.2.1. *Individual effects of circulation, density stratification and cross-shear.* Figure 7 shows the result of a calculation designed to identify the effect of the circulation Γ, density stratification N and cross-shear V_Z on the evolution of the vortex loop. In figure 7 (*a*), a vortex loop with radius r_0 is given a Γ/UD of 0·06 and a D of $2r_0$; the result shows that its motion is along the vortex-ring axis without variation. The calculation was carried out to $\Gamma t/D^2 = 14{\cdot}4$ and figure 7 (*a*) is a view from an angle to the vortex-ring axis.

Figure 7 (*b*) shows the 'collapse' of the long vortex cylinder depicted in figure 5 at the initial time and nine Brunt–Väisälä periods later. The Brunt–Väisälä frequency N is defined as $(g\Delta\rho/\rho_0 r_0)^{\frac{1}{2}} = 0{\cdot}006\,\mathrm{s}^{-1}$ and the circulation Γ and cross-shear V_Z are set to zero. A more detailed discussion of this case will be made in figure 8.

Figure 7 (*c*) shows the 'collapse' of a vortex loop in a cross-shear environment. In this case, $\Gamma = 0$, $N = 0$ while the cross-shear $V_Z = 0{\cdot}003\,\mathrm{s}^{-1}$. Results at $V_Z t = 0$, 1·5 and 4·5 are shown; they indicate a simple stretching along the shear. Owing to this stretching mechanism, we shall find interesting results to be discussed in the following sections.

The collapse of a stratified wake has been a subject of study for some time, the experimental study by Wu (1969) having been the most illustrative one. In figure 8 we show the wake width, or the lateral dimension of the vortex loop, *vs.* time Nt. Wu's experiment was done in a linearly stratified medium while the calculation was performed for a two-layer case which is characterized by the time scale $(g\Delta\rho\pi/\rho_0 r_0)^{\frac{1}{2}}$ and is equivalent to $(g\Delta\rho/\rho_0 r_0)^{\frac{1}{2}} \equiv (g\rho_0^{-1}d\rho_0/dz)^{\frac{1}{2}}$ for a linearly stratified medium. We have transformed Wu's results to conform with the notation used in the calcu-

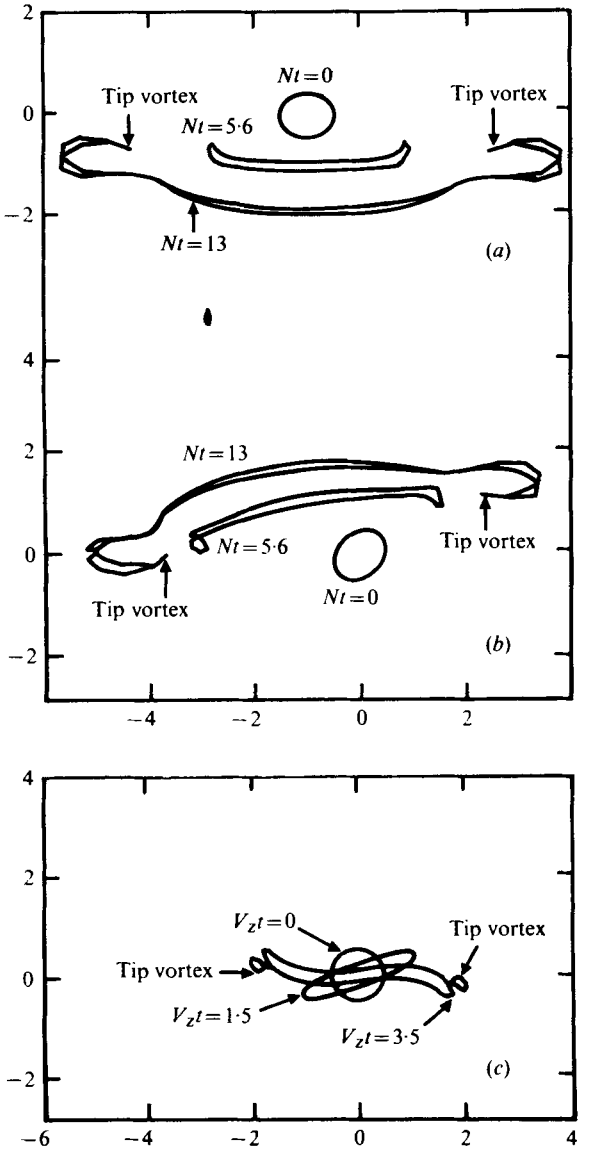

FIGURE 9. Evolution of a vortex ring in a stably stratified medium or a cross-shear environment. The movement of the vortex loop is indicated by the Nt or $V_Z t$ value. (*a*) $\Gamma \neq 0$, $N \neq 0$, $V_Z = 0$, viewed along and from above the vortex-ring axis. (*b*) $\Gamma \neq 0$, $N \neq 0$, $V_Z = 0$, viewed from below the vortex-ring axis. (*c*) $\Gamma \neq 0$, $N = 0$, $V_Z \neq 0$, viewed along the vortex-ring axis.

lation. Fair agreement exists between them, although Wu's result is higher than the calculated result. This may be attributed to the turbulent diffusion, which is not considered in the calculation. Also shown is Kármán's (1940) prediction of the advance velocity of a gravity current, which also agrees reasonably with the calculated result. These comparisons validate the 'numerical experiment as an accurate realization.

3.2.2. *Combined effects of circulation and density stratification or cross-shear.* With the general results shown in the last section in mind, we shall discuss the following two interesting cases in this subsection:

(i) $\Gamma/UD = 0{\cdot}06$, $N = 0{\cdot}006\,\mathrm{s}^{-1}$, $V_Z = 0$, so that $F_D = U/ND = 32$,

(ii) $\Gamma/UD = 0{\cdot}06$, $N = 0$, $V_Z = 0{\cdot}003\,\mathrm{s}^{-1}$, so that $U/V_Z D = 64$.

Figure 9 shows the evolution of the vortex loop for those two cases. Figure 9 (*a*) shows the formation of 'tip vortices' at the two lateral ends at $(Nt)_{\mathrm{tip}} = 13$ after the vortex loop has 'collapsed' at $(Nt)_c = 5{\cdot}6$. At the initial stage of 'collapse' shown in figure 7 (*b*), the vertical height of the centre portion is reduced, so that near there acceleration will take place. Once the opposite sides of the vortex loop fall within the core radius $\bar{r}_c = 0{\cdot}8$, the vorticity is cancelled owing to the solid-body rotation within the core radius. The only surviving component of vorticity is in the vertical direction; the only vorticity is then concentrated at the lateral ends, and the subsequent motion is a simple vortex flow around that vertical vortex. Observation of these 'tip vortices' is reported by Pao & Lin (1973). Conceivably, these large horizontal eddies should also exist in the deep ocean. Figure 9 (*b*) shows the same series, but from a different angle.

Knowing the basic mechanism present for the vortex-loop 'collapse' in a stratified medium and the similar 'collapse' in a shear flow, one can conceive that the formation of 'tip vortices' is also possible in a shear flow. Figure 9 (*c*) shows the vortex-loop evolution in a shear flow. Since the basic time scale in the problem is V_Z^{-1}, the time scale for collapse to take place is about $(V_Z t)_c = 1{\cdot}5$ and for the formation of a tip vortex is $(V_Z t)_{\mathrm{tip}} = 3{\cdot}5$. Notice that $(V_Z t)_{\mathrm{tip}}/(V_Z t)_c \cong (Nt)_{\mathrm{tip}}/(Nt)_c$, which indicates that the basic mechanism is identical in the two cases of 'collapse' and formation of 'tip vortices'.

Another important observation here is that for either case vorticity is 'transferred' from the scale corresponding to the initial vortex-ring dimension to an arbitrarily small scale represented by the tip-vortex dimension, though one should note that, in the numerical experiment, the smallest scale is limited by the core radius $\bar{r}_c$, which is 80 % of the initial ring radius. Still, one can conceive that in reality the vortex loop will cascade into smaller and smaller vortex loops simulated by the 'tip vortices'.

3.2.3. *Combined effect of circulation, density stratification and cross-shear.* When both density stratification and cross-shear are applied to a vortex ring, its evolution is quite complex. Figure 10 shows the result; initially, at $Nt = 0$, the vortex loop is a vortex ring, carrying $\Gamma/UD = 0{\cdot}06$. Also, $N = 0{\cdot}006\,\mathrm{s}^{-1}$ and $V_Z = 0{\cdot}003\,\mathrm{s}^{-1}$, therefore the Richardson number $Ri = (N/V_Z)^2 = 4$ and $F_D = 32$ are specified. The evolution can be demonstrated from three views; figure 10 (*a*) shows a view along the x axis; figures 10 (*b*) and (*c*) show views along the y and z axes. The scales are close but not exactly the same. Figure 10 (*a*) illustrates the vortex-loop rotation as a function of time, at a rate equal to the cross-shear V_Z. The reduction of vertical height is a result of both stable stratification and cross-shear. Formation of tip vortices is apparent at $Nt = 4{\cdot}8$. Rotation of the vortex loop is clearly demonstrated by following the same point P on the vortex loop in figures 10 (*a*), (*b*) and (*c*). One can notice also the 'twisting' motion shown at $Nt = 1{\cdot}3$ and beyond in figures 10 (*b*) and (*c*). This is a result of the Magnus force $\mathbf{f} = -\mathbf{u} \times \boldsymbol{\omega}$, where $\mathbf{u}$ is the local velocity (in this case is primarily the cross-shear velocity) and $\boldsymbol{\omega}$ is the circulation carried along the vortex loop. Figure 11

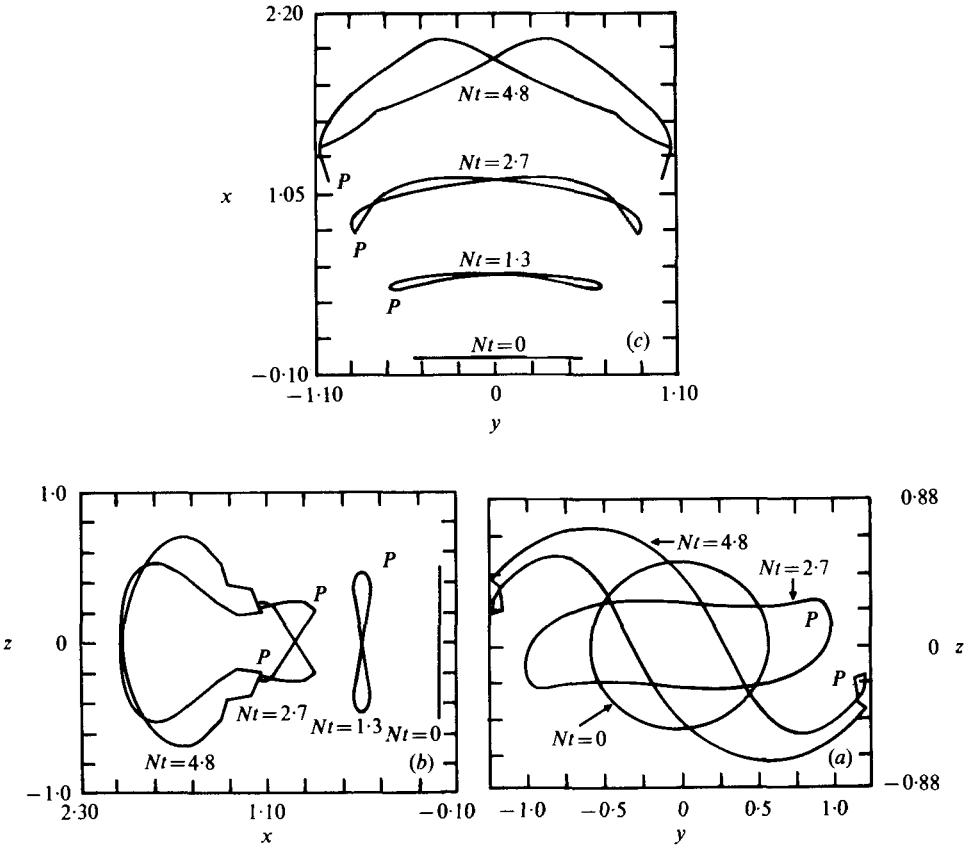

FIGURE 10. Evolution of a vortex loop under the influence of circulation, density stratification and cross-shear. The Richardson number $(N/V_Z)^2 = 4$. (*a*) Viewed along the z axis. (*b*) Viewed along the y axis. (*c*) Viewed along the x axis.

illustrates this force along various parts of the vortex loop. The top and side views show the 'twist' motion imposed on the vortex loop. It is conceivable that severe shear will transform a vortex ring into a 'stellarator' or 'figure of eight' geometry (Kress 1969), as seen at $Nt = 1{\cdot}3$ in figures 10(*b*) and (*c*), in which one vortex loop is essentially divided into two smaller loops.

4. Conclusion

Important observations from this numerical experiment can be summarized as follows.

(i) A stable density stratification destroys all vorticity in the non-vertical direction, so that the surviving vertical vorticity will form the 'horizontal vortices'.

(ii) The effects of cross-shear can be summarized as follows.

(*a*) Cross-shear also 'collapses' a vortex loop and leads to the formation of 'tip vortices'.

(*b*) The Magnus force will 'twist' the vortex loop into a 'figure of eight' geometry

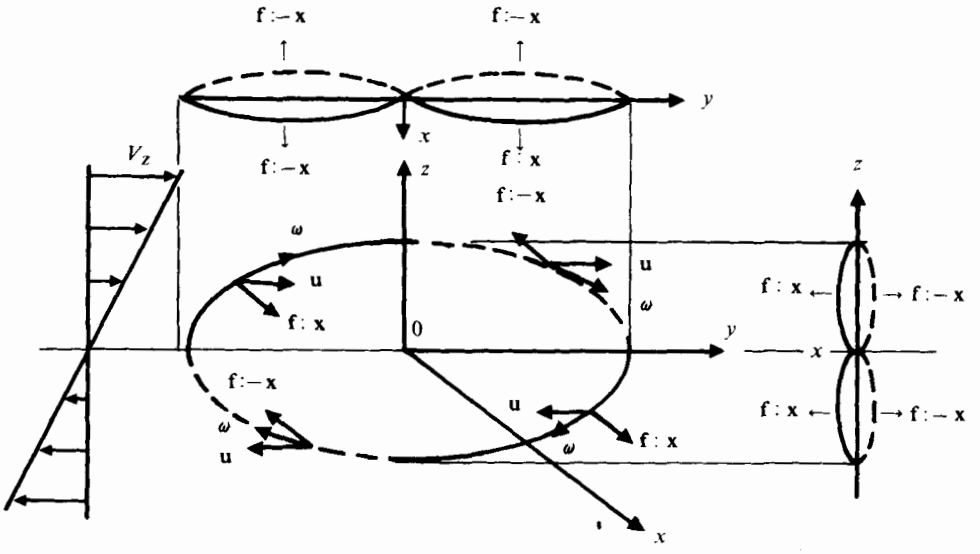

FIGURE 11. The Magnus-force effect of cross-shear on a vortex loop.

and bisect it into two smaller vortex loops which in turn will be bisected into even smaller vortex loops.

(*c*) A vortex loop rotates in a cross-shear at an angular velocity equal to the cross-shear V_Z.

(*d*) Cross-shear is the primary source for both the energy cascading mechanism and generation of turbulence by the conversion of mean-flow vorticity into smaller-scale vortices, i.e. randomization of the mean flow.

This work was sponsored by the internal R & D program within Science Applications, Inc. The author is greatly indebted to Dr William Y. Shaw for his assistance in computer programming. The author also wishes to thank both Dr J. Robert Beyster for his support and Dr Keith J. Victoria for discussions and his constant encouragement.

REFERENCES

CHORIN, A. J. 1973 Numerical study of slightly viscous flow. *J. Fluid Mech.* **57**, 785–796.

FINK, P. T. & SOH, W. K. 1974 Calculation of vortex sheets in unsteady flow and applications in ship hydrodynamics. *Univ. New South Wales Rep.* NAV/ARCH 74/1.

KÁRMÁN, T. VON 1940 The engineer grapples with nonlinear problems. *Am. Math. Soc. Bull.* **46**, 615–683.

KRESS, R. 1969 Treatment of the Prager problem of potential theory by the integral equation method. *Phys. Fluids Suppl.* **12**, II 120–125.

LEONARD, A. 1974 Numerical simulation of interacting, three-dimensional vortex filaments. In *Lecture Notes in Physics*, vol. 35, pp. 245–250. Springer.

PAO, Y. H. & LIN, J. T. 1973 Turbulent wake of a towed slender body in stratified and non-stratified fluids: analysis and flow visualizations. Presentation at *26th Ann. Meeting Fluid Dyn. Div. Am. Phys. Soc.*

ROSENHEAD, L. 1931 The formation of vortices from a surface of discontinuity. *Proc. Roy. Soc.* A **134**, 170–192.

TENNEKES, H. & LUMLEY, J. L. 1972 *A First Course in Turbulence.* M.I.T. Press.

THOMSON, J. A. L. & MENG, J. C. S. 1974 Studies of free buoyant and shear flows by the vortex-in-cell method. In *Lecture Notes in Physics*, vol. 35, pp. 401–416. Springer.

WU, J. 1969 Mixed region collapse with internal wave generation in a density-stratified medium. *J. Fluid Mech.* **35**, 531–544.